

Pressure and Temperature Dependences of the Electronic Structure of CeIrSi₃ Probed by Resonant X-ray Emission Spectroscopy

Hitoshi YAMAOKA¹, Ignace JARRIGE², Naohito TSUJII³, Akio KOTANI^{1,4}, Jung-Fu LIN⁵, Fuminori HONDA⁶, Rikio SETTAI⁶, Yoshichika ŌNUKI⁶, Nozumu HIRAOKA⁷, Hirofumi ISHII⁷, and Ku-Ding TSUEI⁷

¹Harima Institute, The Institute of Physical and Chemical Research (RIKEN), Sayo, Hyogo 679-5148, Japan

²Japan Atomic Energy Agency, SPring-8, Sayo, Hyogo 679-5148, Japan

³Quantum Beam Center, National Institute for Materials Science, Tsukuba, Ibaraki 305-0047, Japan

⁴Photon Factory, Institute of Materials Structure Science, High Energy Accelerator Research Organization, Tsukuba, Ibaraki 305-0801, Japan

⁵Department of Geological Sciences, The University of Texas at Austin, Austin, TX 78712, U.S.A.

⁶Faculty of Science, Osaka University, Toyonaka, Osaka 569-0043, Japan

⁷National Synchrotron Radiation Research Center, Hsinchu 30076, Taiwan

(Received June 28, 2011; accepted September 27, 2011; published online November 2, 2011)

Pressure and temperature dependences of the electronic structure of the heavy-fermion superconductor CeIrSi₃ have been investigated using partial fluorescence yield x-ray absorption spectroscopy and resonant x-ray emission spectroscopy at the Ce L_3 edge. Ce is in a weakly mixed valence state at ambient pressure, mostly f^1 with a small contribution from the f^0 component. Pressure-induced increase of the Ce valence becomes apparent above 4 GPa, concomitantly with the disappearance of the superconductivity. No temperature dependence of the Ce valence is observed within the measured temperature range down to 24 K.

KEYWORDS: electronic structure, Ce, x-ray emission spectroscopy, superconductivity, high pressure

1. Introduction

In some heavy fermion compounds, unconventional superconductivity has been observed at or near the pressure-induced quantum critical point (QCP) between antiferromagnetic (AFM) and non-Fermi liquid ground states.^{1,2)} Accordingly, clarifying the physical properties of these systems around their QCP has recently become a central issue in the f -electron physics.^{3–5)} Recently, pressure-induced superconductivity was found in heavy fermion compounds with no inversion symmetry along the c -axis in the tetragonal crystal structure, such as CePt₃Si,⁶⁾ CeRhSi₃,⁷⁾ and CeIrSi₃.⁸⁾ These compounds, because of their non-centrosymmetric crystal structure, are believed to prevent the realization of the normal spin-singlet superconductivity. Instead, it is considered that mixed cooper pairing between even (d -wave type, spin-singlet) and odd (p - or f -wave type, spin-triplet) parities may occur through the Rashba-type antisymmetric spin-orbit coupling.^{9–14)} In CeIrSi₃, superconductivity occurs at low temperature in the limited pressure range of 1.8–3.3 GPa.^{8,15,16)} The highest superconducting transition temperature, T_C , is 1.6 K at 2.6 GPa, which is relatively high in the family of Ce-based heavy fermion superconductors. The Néel temperature is 5.0 K at ambient pressure and decreases with pressure, resulting in the disappearance of the AFM order at 2.25 GPa, corresponding to the QCP.^{8,16,17)}

The phase transition at the QCP is commonly described by some scenarios including the conventional spin-density-wave (SDW) QCP and the Kondo breakdown at the QCP.^{3,18,19)} In the SDW QCP scenario the Kondo effect is retained with finite Kondo temperature, accordingly a non-integer valence state and a gradual change in the Kondo effect should be observed around the QCP, while in the Kondo-breakdown QCP scenario, a breakdown of the Kondo screening occurs at the QCP^{20–22)} as in CeCu_{6– x} Au _{x} and

YbRh₂Si₂.²³⁾ It appears therefore that the valence and the electronic structure around the QCP may be key factors to understand the mechanism underlying the occurrence of superconductivity and non-Fermi liquid behavior in these materials.

The electronic structure of CeIrSi₃ has been studied by angle-resolved resonant photoelectron spectroscopy (PES) and band calculations in the local density approximation.²⁴⁾ Both experiment and theory suggested that the Ce $4f$ electrons have an itinerant character because of their hybridization with the conduction band c . But under high pressure, where PES is not applicable, the electronic structure of CeIrSi₃ remains unexplored. Since compressed f electrons systems are prone to enhanced c - f hybridization, the question arises as to whether valence fluctuations play a role in the occurrence of superconductivity and non-Fermi liquid behavior around the QCP. This motivated us to investigate the pressure and temperature dependences of the electronic structure of CeIrSi₃ utilizing two photon-in photon-out complementary spectroscopic probes, partial fluorescence yield x-ray absorption spectroscopy (PFY-XAS) and resonant x-ray emission spectroscopy (RXES),^{25–31)} at the Ce L_3 edge. The PFY-XAS and the RXES yield truly bulk-sensitive information about the electronic structure. We examine the pressure dependence of the Ce valence especially around the quantum critical point, which is known to take place around 2.25 GPa where T_N goes to zero while T_C reaches its maximum value. Our results suggest that the onset of the increase of the Ce valence under pressure coincides with the disappearance of superconductivity around 4 GPa. We suggest that the two-dimensional (2D) SDW QCP and the valence QCP scenarios can explain part of the low-temperature properties around the QCP, although an alternative scenario or modification of the scenario may be required for a complete understanding of the QCP physics of CeIrSi₃.

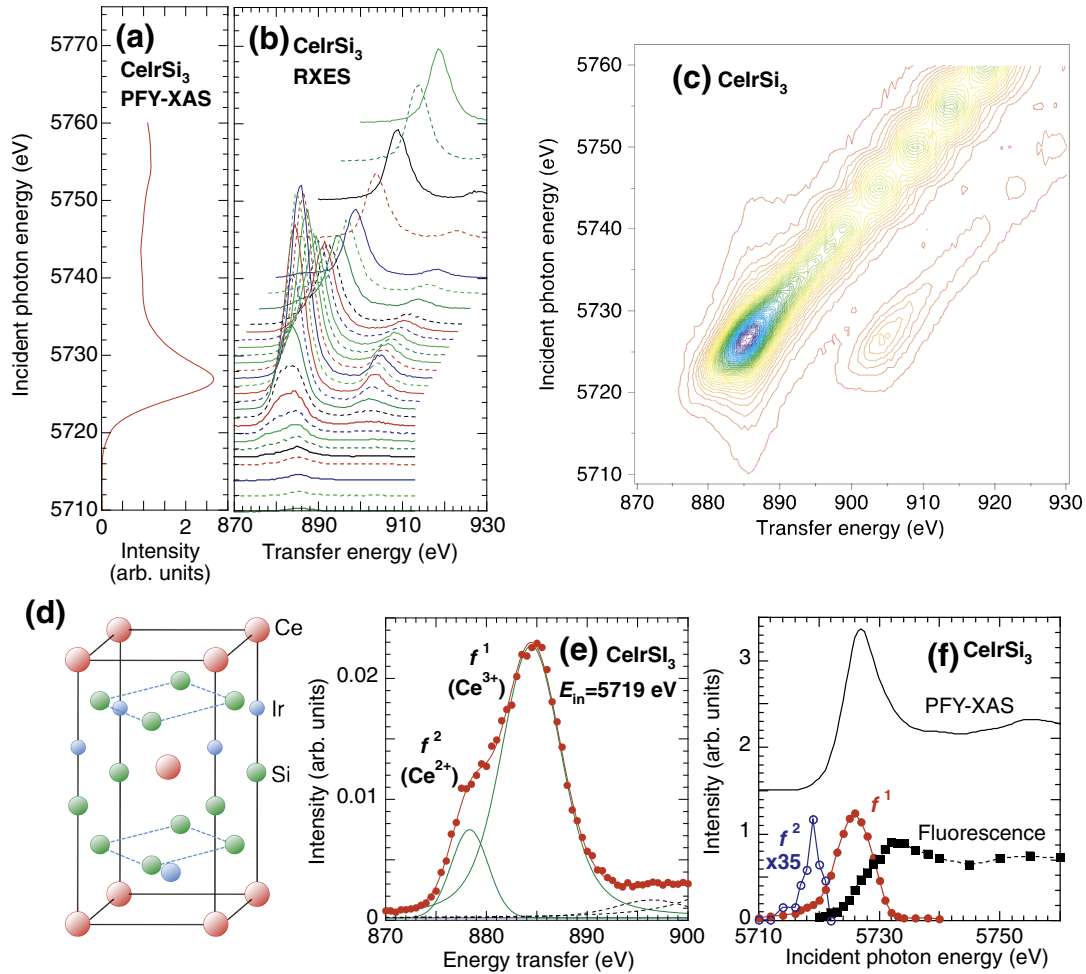


Fig. 1. (Color online) (a) PFY-XAS spectra. (b) RXES spectra as a function of the incident photon energies. The vertical offset of the RXES spectra is scaled to the incident energy axis of the PFY-XAS spectrum. (c) Contour image of the RXES spectra. (d) Crystal structure of CeIrSi_3 . (e) An example of fit of a RXES spectrum, for an incident photon energy $E_{\text{in}} = 5719$ eV. Closed circles are experimental data. (f) Incident energy dependence of the fitted Raman (open circles for f^2 and closed circles for f^1) and fluorescence (closed squares) components. Closed circles are experimental data.

2. Experiment

A single crystal of CeIrSi_3 was synthesized by the Czochralski method in a tetra-arc furnace.¹⁶⁾ The residual resistivity ratio $RRR (= \rho_{\text{RT}}/\rho_0)$ is about 120, where ρ_{RT} and ρ_0 are the resistivity at room temperature and the residual resistivity, respectively. PFY-XAS and RXES measurements were performed at the Taiwan beamline BL12XU at SPring-8. The undulator beam was monochromatized by a pair of Si(111) crystals and focused to a size of 30 (horizontal) \times 20 (vertical) μm^2 at the sample position using a toroidal and K-B mirrors. Incident photon energies are calibrated by using metal K -absorption edges of V and Cr. The incident photon flux was estimated to be about $(7\text{--}8) \times 10^{11}$ photons/s at 5.46 keV. A Johann-type spectrometer equipped with a spherically bent Si(400) crystal (radius of about 1 m) was used to analyze the $\text{Ce } L\alpha_1$ ($3d_{5/2} \rightarrow 2p_{3/2}$) emission line with a solid state detector (XFlash 1001 type 1201). The overall energy resolution was estimated to be about 1.5 eV around the emitted photon energy of 4.8 keV. The intensities of all spectra are normalized by the incident beam intensity monitored just before the sample. A closed-circuit He cryostat was used for the low-temperature measurements down to 24 K. The high-

pressure conditions were realized using a diamond anvil cell (DAC) with a Be-gasket. We used the in-plane geometry where both the incoming and outgoing beams go through the Be gasket, with a scattering angle of 90° . The pressure-transmitting medium was silicone oil. The pressure was measured based on the Raman shift of the fluorescence from tiny ruby balls in the DAC.

3. Results

3.1 RXES

Figure 1(a) shows the PFY-XAS spectrum measured at the Ce L_3 edge at room temperature. In Fig. 1(b), the incident energy dependence of the corresponding RXES spectra is plotted as a function of the energy transfer (E_{tr}), defined as the difference between the incident and emitted photon energies. The vertical offset of the RXES spectra in Fig. 1(b) is scaled to the incident energy axis of the PFY-XAS spectrum. Two Raman components respectively corresponding to Ce^{2+} ($E_{\text{tr}} \simeq 878$ eV) and Ce^{3+} ($E_{\text{tr}} \simeq 886$ eV) are clearly observed in the RXES spectra below the absorption edge. Contour intensity map is shown in Fig. 1(c). When increasing the incident energy above the edge, the Raman signal disappears at the expense of two fluorescence components, attributed to the $L\alpha_1$ and $L\alpha_2$

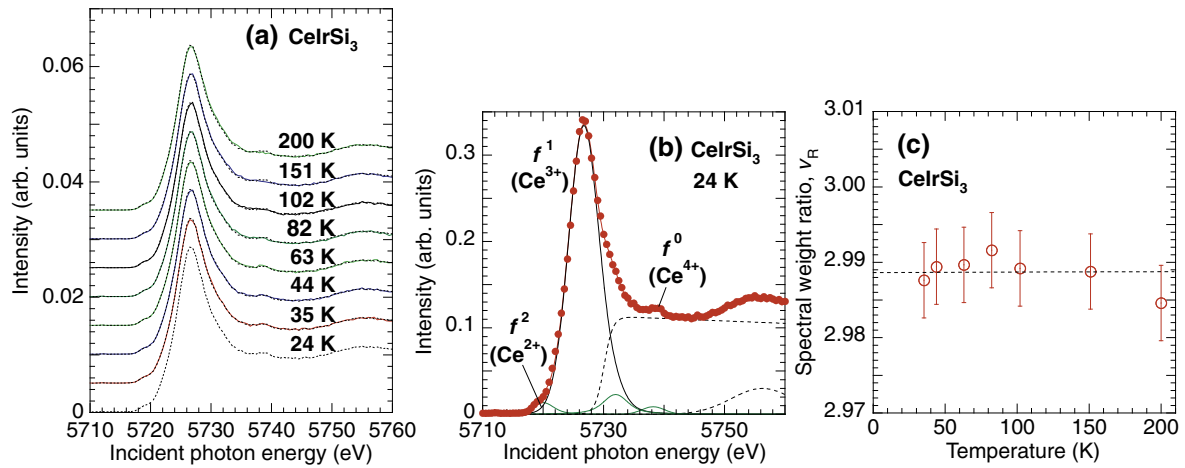


Fig. 2. (Color online) (a) Temperature dependence of the PFY-XAS spectrum at ambient pressure. Each spectrum between 35 and 200 K (solid line) is compared to the spectrum at 24 K (dotted line). (b) Example of fit of the PFY-XAS spectrum, at 24 K. Closed circles are the experimental data. (c) Temperature dependence of the estimated spectral weight ratio (v_R). Dashed line corresponds to mean value.

lines, which appear at constant emitted photon energy, i.e., the fluorescence energies are proportional to E_{tr} . Figure 1(d) shows the crystal structure of CeIrSi₃. In order to extract the relative intensity of each f component we have fitted the PFY-XAS and RXES spectra.^{25–31} For the fit of the RXES spectra, we used two Voigt functions for f^1 and f^2 , as shown in Fig. 1(e). The incident energy dependence of the intensities of the Raman 2+ and 3+ components and the fluorescence, as estimated from the fits, is plotted in Fig. 1(f) along with the PFY-XAS spectrum. The weak Ce²⁺ component is successfully separated from the main Ce³⁺ component. It is noted that in core-level spectroscopy there is a dynamical screening effect caused by the core-hole potential in the final excited state. A charge transfer between the ligand and the excited atom can occur, therefore the measured spectra do not necessarily correspond to the ground state.^{31,32} In Ce compounds the final-state effect mainly results in an increase of the f^2 component, while the hybridization affects the f^0 and f^1 components. Here we define the spectral weight ratio (v_R), which correlates with the mean valence in the ground state (v_g), as $v_R = 3 + [I(f^0) - I(f^2)]/[I(f^0) + I(f^1) + I(f^2)]$, where $I(f^n)$ is the intensity of the f^n component. The ratio v_R is estimated to be 2.985 ± 0.010 from our room-temperature RXES spectra. In the fits of the RXES spectra, we ignore the $4f^0$ component, which is too weak to be discriminated from the intense fluorescence peak. We are however able to extract the $4f^0$ component in the PFY-XAS spectra, as shown below, which results in slightly different values of v_R compared with RXES.

3.2 Temperature dependence

Figure 2 shows the temperature dependence of (a) the PFY-XAS spectra and (c) the estimated spectral weight ratio. In Fig. 2(b) an example of fit of the PFY-XAS spectrum is shown. The PFY-XAS spectrum consists of two weak features of Ce²⁺ ($4f^2$) at $E_{in} = 5719$ eV and Ce⁴⁺ ($4f^0$) at $E_{in} = 5738$ eV, and a strong Ce³⁺ ($4f^1$) component at $E_{in} \simeq 5727$ eV, where E_{in} is the incident photon energy, indicating that CeIrSi₃ is in a mixed valence state. The presence of the ($4f^0$) component points to a finite c - f

hybridization, which is consistent with the itinerant character of the $4f$ electrons concluded from a comparison of angle-resolved PES results with local density approximation calculations.²⁴ In the fits, after subtraction of an arctangent-like (asymmetrical double sigmoid) function corresponding to the continuum excitations, three Voigt functions are used to fit the f^0 , f^1 , and f^2 components. We note that the mean value of v_R in Fig. 2(c) at ambient pressure is slightly different with the values in Fig. 3(b) as will be shown below. This suggests that the absolute value of v_R depends on the sample or measurement conditions, such as having the sample in or out of the high-pressure cell. The reproducibility of the relative changes in v_R upon variation of pressure was nonetheless checked and ensured.

3.3 Pressure dependence

The pressure dependence of the PFY-XAS spectra at 300 K is shown in Fig. 3(a). Each spectrum is normalized in intensity by its area after subtracting a constant background. The expanded view of the f^0 component is also shown in Fig. 3(a). With increasing pressure, the intensity of the f^1 -related peak clearly decreases while that of the f^0 -related peak slightly increases. This points to an increase of the c - f hybridization with pressure. The same trend was theoretically suggested for Ce³³ and experimentally observed in the iron pnictide superconductor CeFeAsO_{1-y}.³⁴ The results of the fit of the pressure-dependent PFY-XAS spectra is shown in Fig. 3(b). The ratio v_R is found to slightly increase with pressure above 4 GPa. For comparison, the pressure dependence of the Néel temperature (T_N) and T_C from the literature⁸) are shown in Fig. 3(c).

Here we note that the presence of the f^2 component is mostly related to a final-state effect with a core-hole in the $3d_{5/2}$ level,^{31,35} whereas in the ground state the weight of the f^2 component should be negligibly small.³² Accordingly, the value of the v_R ratio is not exactly the same as v_g and this is discussed in the Appendix. Especially, the fact that v_R is smaller than 3 is due to the presence of the Ce²⁺ component, similarly to CeRu₂Si₂.³⁶ Our result points to an increase of the valence fluctuations with pressure, especially in the 5–8 GPa range. While our high-pressure study for CeIrSi₃

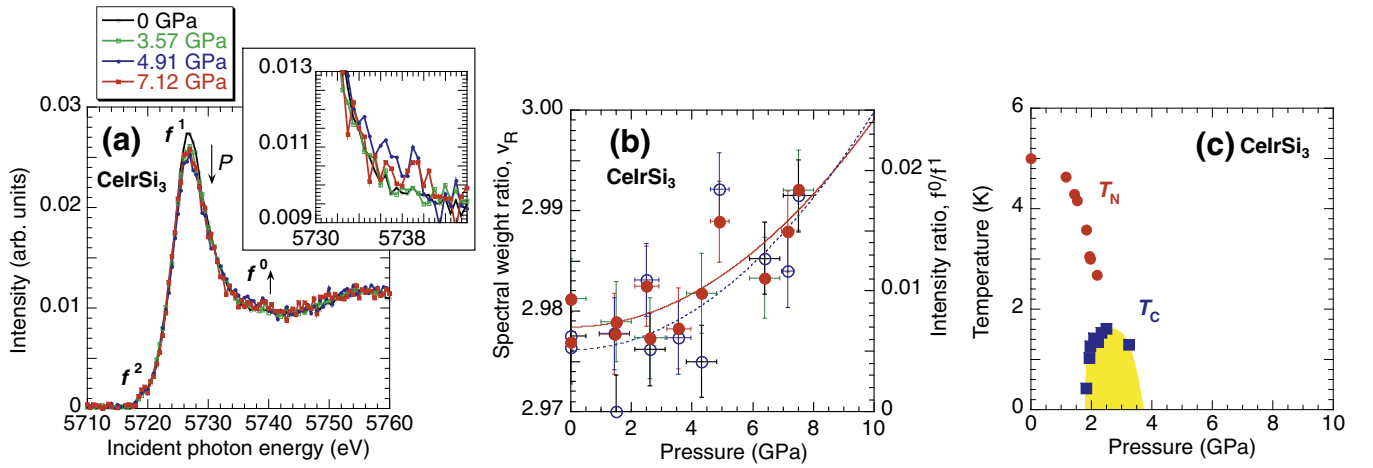


Fig. 3. (Color online) (a) Examples of pressure dependence of the PFY-XAS spectra normalized by the area. Upper-right panel is expanded view of the f^0 component for the five-point smoothed data. (b) Pressure dependence of the estimated spectral weight ratio (closed circles, v_R) and intensity ratio of f^0 to f^1 (open circles). Solid and dashed lines are quadratic-function fits of v_R and the f^0/f^1 ratio, respectively. (c) Néel transition (closed circles, T_N) and superconducting transition (closed squares, T_C) temperatures as a function of pressure. Data in (c) are taken from the literature.⁸⁾

was performed at room temperature, one may expect a similar pressure dependence of the valence at low temperature since no temperature dependence of the valence is observed at ambient pressure.

4. Discussion

4.1 Temperature independence of Ce valence

Almost no temperature dependence is observed for v_R in the measured temperature range down to 24 K within our measurement accuracy. The single impurity Anderson model (SIAM), which is described by the single energy scale of the Kondo temperature (T_K), is normally applicable to the Ce or Yb valence fluctuating systems.^{30,37)} In the SIAM picture the valence becomes temperature dependent below T_K . However, in CeIrSi₃ we should consider the crystal electric field (CEF) which was estimated to be 160 and 501 K for the first and second excited states.⁸⁾ In the single ion impurity picture the relation between the Kondo temperature and the 4*f* occupation number (n_f) is written to be

$$\frac{n_f}{1 - n_f} = N(\epsilon_F) N_f V^2 \sum_m \frac{1}{k_B T_K + \Delta_m}, \quad (1)$$

where ϵ_F , $N(\epsilon_F)$, N_f , V , k_B , and Δ_m are the Fermi level, the density of states at ϵ_F , the degeneracy of the 4*f* states, the hybridization strength, the Boltzmann constant, and the CEF excitation energy, respectively.^{35,38–40)} In Ce systems the 4*f* occupation n_f can be expressed as $n_f = 4 - v_g$. For $T_K \ll \Delta_m$ the effect of the Kondo temperature is small. We can make a rough estimation of T_K using the formulas based on the Coqblin–Schrieffer model, $T_K \simeq 1.29T_0$ ⁴¹⁾ and $T_0 = N_A(v - 1)\pi k_B/6\gamma$,⁴²⁾ where T_0 , N_A , v , and γ are the characteristic temperature, the Avogadro's number, the degeneracy, and the electronic specific coefficient, respectively. T_K is estimated to be on the order of ~ 45 K, which is smaller than the 100 K estimated by resistivity.¹⁵⁾ Either way, T_K is smaller than the 160 K of Δ_m in CeIrSi₃. Equation (1) does not show temperature dependence of n_f directly, but it suggests that n_f is mainly determined by the CEF and the hybridization effect at $T \leq T_K$ is small when

the CEF is much larger than T_K . This may explain the absence of temperature dependence of v_R for CeIrSi₃.

4.2 Ce valence and superconductivity

The interaction (J) between the localized electron spin and the conduction electrons is described by the relation $J = N_f V^2 / |\epsilon_f|$, where $|\epsilon_f|$ is the position of the 4*f* states relative to the Fermi level.⁴³⁾ In the Ce systems the 4*f* level is lower than the Fermi level. An increase in pressure will raise the 4*f* level of the Ce³⁺ component which thus approaches ϵ_F . This results in a decrease of $|\epsilon_f|$, and therefore an increase of J . Small changes in J cause drastic changes in the Kondo effect because the Kondo temperature (T_K) exponentially increases with J following the relation $T_K \propto \exp\{-1/[N(\epsilon_F)J]\}$. The pressure dependence of v_R in CeIrSi₃ is typical for Ce compounds, as it reflects an increase in the valence, i.e., the hybridization, with pressure.^{34,44)} Accordingly, one may expect T_K to increase under pressure, which is in concordance with the reported pressure-induced decrease of T_N . This is in line with the general view that the QCP corresponds to the hybridization-mediated transition from a magnetic ground state dominated by the Ruderman–Kittel–Kasuya–Yosida (RKKY) interaction, to the Kondo effect-driven non-magnetic ground state. However, the coexistence suggested by our study between weak valence fluctuations, where the deviation from the integer valence is much less than 0.1, pointing to a rather itinerant character of the 4*f* electrons and AFM order is more unusual. Finally, the Ce⁴⁺ (f^0) component seemingly increases for pressures above the QCP, signifying an increase of the *c*–*f* hybridization and an exponential increase of T_K . Accordingly, the valence starts to increase above 4 GPa, coinciding with the reported decline of T_C , while the valence fluctuations remain weak in the pressure region where superconductivity occurs. This suggests that the decrease of T_C , and ultimately the disappearance of the superconducting state, may be induced by the concomitant pressure-induced increase of the valence fluctuations.

An important remaining factor about the occurrence of superconductivity in CeIrSi₃ is the lack of inversion

symmetry in the crystal structure. In our x-ray spectroscopic study, however, it is not clear how the lack of inversion symmetry affects the electronic structure and the valence. In contrast to CeIrSi₃, CeMIn₅ ($M = \text{Co, Rh}$) has an inversion symmetry.¹¹ A comparative measurement of the electronic and crystal structures as a function of pressure for both CeIrSi₃ and CeMIn₅ may therefore be of interest.

4.3 Ce valence and hybridization strength

Specific heat data of CeIrSi₃ showed a small entropy of $0.2R \ln 2$, which may be caused by the Kondo effect.¹⁶ This is consistent with the itinerant character of the $4f$ electrons showed by PES.²⁴ We note that the itinerant character of the $4f$ electrons had also been pointed out for CeRu₂Si₂, for which the f^0 and f^1 intensities are respectively slightly higher and lower compared with CeRu₂Ge₂.³⁶ Thus a small increase in the hybridization between CeRu₂Ge₂ and CeRu₂Si₂ was suggested to result in a drastic difference between their electronic specific coefficient (γ), ~ 350 mJ/(mol·K²) for CeRu₂Si₂, 20 times larger than for CeRu₂Ge₂. Drawing a parallel with CeIrSi₃, the high γ value of about 120 mJ/(mol·K²) and the f^0 component detected by PFY-XAS may reflect the presence of finite hybridization at ambient pressure. Now, there remains a general open question about compressed Ce systems; why do the valence fluctuations remain weak in the low pressure region although the $4f$ electrons already exhibit an itinerant character at ambient pressure? To consider this problem quantitatively, we return to eq. (1). In this relation if the Ce valence state is pure Ce³⁺ ($n_f = 1$), the left side of eq. (1) is infinite, corresponding to $T_K = 0$. While, if the Ce valence is Ce⁴⁺ ($n_f = 0$), the left side of eq. (1) goes to zero, corresponding to diverging- T_K . Under large $N(\epsilon_F)N_f V^2 / k_B T_K$ condition n_f becomes insensitive to the change in T_K . Therefore in Ce system the left side of eq. (1) should keep larger value even when T_K changes, which corresponds to the Ce state close to Ce³⁺. This may be a reason why the changes in the Ce valence remain small at low pressures. However, T_K increasing exponentially under pressure, n_f is bound to deviate from 1 above a given pressure, which is around 4–5 GPa for CeIrSi₃ as shown in Fig. 3(b). More qualitative explanation can be found in the Appendix.

4.4 Ce valence and QCP

We first use resistivity, magnetic, and nuclear magnetic resonance (NMR) data from the literature to discuss the possible scenarios for the QCP in CeIrSi₃, and then continue the discussion in view of our results. At ambient pressure the resistivity shows T^2 dependence at $T < 2$ K, indicating Fermi liquid state. The Néel temperature decreases with pressure, resulting in the disappearance of the AFM order at the QCP.^{8,16,17} At 2.5 GPa a T -linear temperature dependence of the resistivity was observed below $T = 18$ K,^{11,16} pointing to a non-Fermi liquid state. Thus, as pressure is increased the superconducting state is seen to coexist successively with AFM order and non-Fermi liquid behavior.⁴⁵ Such coexistence of the AFM order and the superconductivity was also observed in CePd₂Si₂.¹ As mentioned above, the phase transition at the QCP can usually be described either by the SDW-QCP scenario or by the Kondo-breakdown QCP scenario.^{3,20–22} The Kondo-

breakdown QCP scenario^{3,20} also predicts that the $1/T_1$ ratio in NMR is constant at low temperature around the QCP,⁴⁶ which was shown not to be the case.⁴⁵ Therefore the Kondo-breakdown scenario should be ruled out in CeIrSi₃.

We now consider the SDW QCP scenario, or rather the AFM-SDW QCP scenario, as in CeIrSi₃ the AFM order merges with the superconducting region around the QCP. However, the T -linear dependence of the resistivity near the QCP cannot be explained by the 3-D AFM-SDW QCP which predicts a $T^{3/2}$ -dependence of the resistivity.¹⁹ On the other hand, the nuclear spin lattice relaxation rate ($1/T_1$) in NMR shows a $T^{1/2}$ dependence near the QCP,⁴⁵ which supports the 2D AFM-SDW QCP. However, we note that no sign of occurrence of SDW anomaly was found in a previous resistivity measurement up to 10 K.¹⁶

Watanabe and Miyake proposed a theory to explain the physical properties around the QCP in CeRhIn₅, whose originality is to take into account the Ce valence fluctuations and their interplay with the magnetic order (valence QCP scenario).⁴⁷ They succeeded to obtain the enhancement of the electron effective mass by keeping finite c - f hybridization and T -linear resistivity around the QCP. Valence-fluctuation mediated superconductivity was also suggested, where the Coulomb repulsion between f and conduction electrons causes the valence transition.^{4,48,49} According to the corresponding theory, superconductivity develops just before the valence crossover, where a small change in the valence on the order of 0.01 may occur.⁵⁰ The mixed valence and change in the Kondo effect around the QCP are in favor of such a scenario, as recently discussed in CeCu₂Si₂.⁴⁴ Further evidence comes from the fact that the Ce valence remains nearly constant as pressure is increased throughout the superconducting regime, and starts increasing around 4 GPa where superconductivity terminates. Therefore, based on our results, it seems that it is adequate to use the valence QCP scenario to address the occurrence of superconductivity in CeIrSi₃ under pressure. Nonetheless, the consistency of this scenario with other physical properties than resistivity and valence is still unknown.

Finally we also note that we have observed non-integer Yb valences around the QCP of Yb Kondo systems such as YbCu_{5-x}Al_x³⁰ and YbNi₂Ge₂.⁵ For these compounds too, a theoretical description of the physics around the QCP may require the inclusion of the Yb valence fluctuations. Further study is however necessary to determine whether the valence QCP scenario can be used for these compounds, or whether another alternative scenario should be considered.

5. Conclusion

We have studied pressure and temperature dependences of the bulk electronic structure of CeIrSi₃ using PFY-XAS and RXES. CeIrSi₃ is in a weakly mixed valence state at ambient pressure, with the main component f^1 (Ce³⁺) and a small fraction of f^0 (Ce⁴⁺). This suggests that the f electrons have a rather itinerant character, in agreement with a previous study using angle-resolved PES. We did not detect any temperature dependence of the valence down to 24 K at ambient pressure. Under pressure, changes in the spectral weight ratio or valence are very small up to the QCP at 4 GPa, and become more noticeable above 4 GPa, where the superconductivity disappears. This invokes the possibility

that the increase of the valence fluctuations under pressure plays a key role in the the occurrence or extinction of the superconductivity. Both the 2D AFM-SDW QCP and the valence QCP scenarios adequately account for some of the physical properties of CeIrSi₃ around its QCP, although an alternative scenario or modification of the scenario may be required for consistency with the other physical properties.

Acknowledgments

The experiments were performed at Taiwan beamline BL12XU (under SPring-8 Proposals No. 2009B4251 and No. 2009B4266) at SPring-8. We thank Tetsuo Okane and Shinichi Fujimori for useful discussion. This work is partly supported by Grants in Aid for Scientific Research (Grant No. 22540343 and No. 90029504) from the Japan Society for the Promotion of Science and by Murata Science Foundation (Grant No. A04132). J.F.L. acknowledges support from the Energy Frontier Research under Extreme Environments (EFree), the US National Science Foundation (EAR-0838221) and the Carnegie/DOE Alliance Center (CDAC).

Appendix

Here we discuss the relation between the valence number v_R estimated from the PFY-XAS spectra and that in the ground state (denoted by v_g). If the final state interaction in PFY-XAS can be disregarded, v_R should be the same as v_g , but in CeIrSi₃ we show that the final state interaction causes some difference between them.

We consider the SIAM^{35,51,52)} consisting of the Ce 4*f* and conduction band states which are mixed by the hybridization V . We assume that the conduction band is half-filled and its density of states is of rectangular shape with the band width W . For the 4*f* states we take into account only the states with the total angular momentum $J = 5/2$, for simplicity, and the 4*f* level is defined by ϵ_f . The Coulomb interaction between 4*f* electrons is denoted by U_{ff} . If we assume that U_{ff} is infinitely large, the Kondo temperature T_K is calculated in the lowest order approximation of the $1/N_f$ expansion method³⁵⁾ (degeneracy $N_f = 2J + 1 = 6$ for Ce) from the following equation:⁵³⁾

$$k_B T_K - \epsilon_f + \frac{N_f V^2}{W} \left[\log(k_B T_K) - \log\left(k_B T_K + \frac{W}{2}\right) \right] = 0, \quad (\text{A}\cdot 1)$$

and if we obtain T_K , v_g is given by

$$v_g = 4.0 - n_f = 4.0 - \frac{N_f V^2}{2k_B T_K \left(k_B T_K + \frac{W}{2}\right) + N_f V^2}. \quad (\text{A}\cdot 2)$$

In eq. (A.2) when $k_B T_K \ll W$, we obtain the equation

$$\frac{n_f}{1 - n_f} = \frac{N_f V^2}{k_B T_K W} = \frac{N(\epsilon_f) N_f V^2}{k_B T_K}, \quad (\text{A}\cdot 3)$$

where $N(\epsilon_f) = 1/W$. This is the case when the crystal field effect is disregarded in eq. (1). In eq. (A.1) when $k_B T_K \ll W$ and $k_B T_K \ll |\epsilon_f|$, eq. (A.1) is written as

$$-\epsilon_f + \frac{N_f V^2}{W} \log\left(\frac{2k_B T_K}{W}\right) = 0. \quad (\text{A}\cdot 4)$$

Then we can obtain

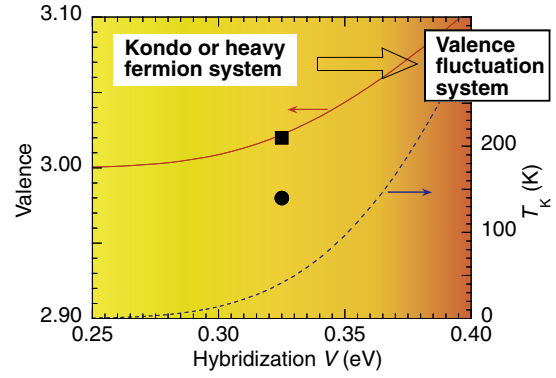


Fig. A-1. (Color online) Calculated results of the valence number v_g in the ground state (solid line) and the Kondo temperature T_K (dashed line) as a function of the hybridization strength V by assuming $U_{ff} = \infty$. For $U_{ff} = 5.0$ eV and $V = 0.325$ eV, the values of v_g and v_R are shown with closed square and closed circle, respectively, where v_R is the valence number in the final state of PFY-XAS. As the V increases the system changes from Kondo or heavy fermion to valence fluctuation system.

$$k_B T_K = \frac{W}{2} \exp\left[-\frac{|\epsilon_f|}{N(\epsilon_f) N_f V^2}\right] = \frac{W}{2} \exp\left[-\frac{1}{N(\epsilon_f) J}\right], \quad (\text{A}\cdot 5)$$

where $J = N_f V^2 / |\epsilon_f|$.

We calculate T_K and v_g as a function of V , and show the results with solid (red) and dashed (blue) lines in Fig. A-1. In these calculations, we take $W = 4.0$ eV and $\epsilon_f = -1.0$ eV measured from the Fermi level. These values are standard ones for mixed valence Ce compounds, though they are not optimized for CeIrSi₃. Since the value of T_K is estimated to be about 45 K in the text of this paper, the value of V is estimated to be about 0.325 and the value of v_g is about 3.02 from Fig. A-1. In Fig. A-1 relatively small hybridization strength region of 0.25–0.3 eV and larger V region of $V \geq 0.4$ eV correspond to typical Kondo system or heavy Fermion system and valence fluctuation system, respectively. We note that when V changes from 0.25 to 0.3 eV, T_K does from 0.5 to 15 K, while the change in the valence is only 0.01. In the valence fluctuation region the valence changes largely with V .

Now we calculate the values of v_R and v_g for $V = 0.325$ eV by taking into account a finite value of U_{ff} . We take $U_{ff} = 5.0$ eV, and introduce the $2p$ core hole potential acting on the 4*f* states $U_{fc} = 10.5$ eV, as well as the Coulomb interaction between the 4*f* and 5*d* electrons $U_{fd} = 1.0$ eV. The calculated $v_R (= 2.98)$ and $v_g (= 3.02)$ are plotted with closed square and closed circle in Fig. A-1, respectively. Note that v_R is smaller than 3.0 while v_g is larger than 3.0. The weights of the f^0 , f^1 , and f^2 configurations in the final state of PFY-XAS are 2.62, 92.4, and 4.94%, respectively, which are in good agreement with Fig. 2(b) of the text. Those values in the ground state are 3.28, 95.5, and 1.15%, respectively. From this result, we see that the f^2 weight is enhanced in the final state of PFY-XAS because of the charge transfer from f^0 and f^1 configurations to the f^2 configuration caused by the creation of the core-hole (final state interaction). Therefore, v_g and v_R are closely related: We can obtain v_g from v_R by transfer 3.8% f^2 weight to f^1 and f^0 weights (3% to f^1 and 0.8% to f^0).

We do not perform similar calculations for the system under pressure, but the situation (the weights of the charge transfer between the ground and final states) should be more or less the same. Therefore we conclude that v_g is always larger than 3.0 and increases with pressure. Theoretical calculations of the PFY-XAS and RXES spectra are left in future investigations.

- 1) N. D. Mathur, F. M. Grosche, S. R. Julian, I. R. Walker, D. M. Freye, R. K. W. Haselwimmer, and G. G. Lonzarich: *Nature* **394** (1998) 39.
- 2) H. Hegger, C. Petrovic, E. G. Moshopoulou, M. F. Hundley, J. L. Sarrao, Z. Fisk, and J. D. Thompson: *Phys. Rev. Lett.* **84** (2000) 4986.
- 3) A. Schröder, G. Aeppli, R. Coldea, M. Adams, O. Stockert, H. v. Löhneysen, E. Bucher, R. Ramazashvili, and P. Coleman: *Nature* **407** (2000) 351.
- 4) A. T. Holmes, D. Jaccard, and K. Miyake: *J. Phys. Soc. Jpn.* **76** (2007) 051002.
- 5) H. Yamaoka, I. Jarrige, N. Tsujii, J.-F. Lin, M. Hiraoka, H. Ishii, and K.-D. Tsuei: *Phys. Rev. B* **82** (2010) 035111.
- 6) E. Bauer, G. Hilscher, H. Michor, C. Paul, E. W. Scheidt, A. Griбанov, Y. Seropugin, H. Noël, M. Sigrist, and P. Rogl: *Phys. Rev. Lett.* **92** (2004) 027003.
- 7) N. Kimura, K. Ito, K. Saitoh, Y. Umeda, and H. Aoki: *Phys. Rev. Lett.* **95** (2005) 247004.
- 8) I. Sugitani, Y. Okuda, H. Shishido, T. Yamada, A. Thamizhavel, E. Yamamoto, T. D. Matsuda, Y. Haga, T. Takeuchi, R. Settai, and Y. Ōnuki: *J. Phys. Soc. Jpn.* **75** (2006) 043703.
- 9) S. K. Yip: *Phys. Rev. B* **65** (2002) 144508.
- 10) P. A. Frigeri, D. F. Agterberg, A. Koga, and M. Sigrist: *Phys. Rev. Lett.* **92** (2004) 097001.
- 11) R. Settai, T. Takeuchi, and Y. Ōnuki: *J. Phys. Soc. Jpn.* **76** (2007) 051003.
- 12) R. Settai, Y. Miyauchi, T. Takeuchi, F. Lévy, I. Shekin, and Y. Ōnuki: *J. Phys. Soc. Jpn.* **77** (2008) 073705.
- 13) T. Kawai, H. Muranaka, M.-A. Measson, T. Shimoda, Y. Doi, D. Matsuda, Y. Haga, G. Knebel, G. Lapertot, D. Aoki, J. Flouquet, T. Takeuchi, R. Settai, and Y. Ōnuki: *J. Phys. Soc. Jpn.* **77** (2008) 064716.
- 14) C. Pfeleiderer: *Rev. Mod. Phys.* **81** (2009) 1551.
- 15) Y. Muro, D. Eom, N. Takeda, and M. Ishikawa: *J. Phys. Soc. Jpn.* **67** (1998) 3601.
- 16) Y. Okuda, Y. Miyauchi, Y. Ida, Y. Takeda, C. Tonohiro, Y. Oduchi, T. Yamada, N. D. Dung, T. D. Matsuda, Y. Haga, T. Takeuchi, M. Hagiwara, K. Kindo, H. Harima, K. Sugiyama, R. Settai, and Y. Ōnuki: *J. Phys. Soc. Jpn.* **76** (2007) 044708.
- 17) N. Tateiwa, Y. Haga, T. D. Matsuda, S. Ikeda, E. Yamamoto, Y. Okuda, Y. Miyauchi, R. Settai, and Y. Ōnuki: *J. Phys. Soc. Jpn.* **76** (2007) 083706.
- 18) T. Moriya and T. Takimoto: *J. Phys. Soc. Jpn.* **64** (1995) 960.
- 19) G. R. Stewart: *Rev. Mod. Phys.* **73** (2001) 797.
- 20) P. Gegenwart, Q. Si, and F. Steglich: *Nat. Phys.* **4** (2008) 186.
- 21) C. Pepin: *Phys. Rev. B* **77** (2008) 245129.
- 22) K.-S. Kim: *Phys. Rev. Lett.* **104** (2010) 156403.
- 23) S. Friedemann, T. Westerkamp, M. Brando, N. Oeschler, S. Wirth, P. Gegenwart, C. Krellner, C. Geibel, and F. Steglich: *Nat. Phys.* **5** (2009) 465.
- 24) T. Ohkochi, T. Toshimitsu, H. Yamagami, S.-i. Fujimori, A. Yasui, Y. Takeda, T. Okane, Y. Saitoh, A. Fujimori, Y. Miyauchi, Y. Okuda, R. Settai, and Y. Ōnuki: *J. Phys. Soc. Jpn.* **78** (2009) 084802.
- 25) I. Jarrige, H. Ishii, Y. Q. Cai, J.-P. Rueff, C. Bonnelle, T. Matsumura, and S. R. Shieh: *Phys. Rev. B* **72** (2005) 075122.
- 26) H. Yamaoka, M. Taguchi, A. M. Vlaicu, H. Ohashi, Y. Yokoi, D. Horiguchi, T. Tochio, Y. Ito, K. Kawatsura, K. Yamamoto, A. Chainani, S. Shin, M. Shiga, and H. Wada: *J. Phys. Soc. Jpn.* **75** (2006) 034702.
- 27) H. Yamaoka, N. Tsujii, K. Yamamoto, H. Ohashi, A. M. Vlaicu, K. Kunitani, K. Uotani, D. Horiguchi, T. Tochio, Y. Ito, and S. Shin: *Phys. Rev. B* **76** (2007) 075130.
- 28) H. Yamaoka, H. Ohashi, I. Jarrige, T. Terashima, Y. Zou, H. Mizota, S. Sakakura, T. Tochio, Y. Ito, E. Ya Sherman, and A. Kotani: *Phys. Rev. B* **77** (2008) 045135.
- 29) H. Yamaoka, N. Tsujii, K. Yamamoto, A. M. Vlaicu, H. Ohashi, H. Yoshikawa, T. Tochio, Y. Ito, A. Chainani, and S. Shin: *Phys. Rev. B* **78** (2008) 045127.
- 30) H. Yamaoka, I. Jarrige, N. Tsujii, N. Hiraoka, H. Ishii, and K.-D. Tsuei: *Phys. Rev. B* **80** (2009) 035120.
- 31) H. Yamaoka, H. Sugiyama, Y. Kubozono, A. Kotani, R. Nouchi, A. M. Vlaicu, H. Ohashi, T. Tochio, Y. Ito, and H. Yoshikawa: *Phys. Rev. B* **80** (2009) 205403.
- 32) H. Yamaoka, A. Kotani, Y. Kubozono, A. M. Vlaicu, H. Ohashi, T. Tochio, Y. Ito, and H. Yoshikawa: *J. Phys. Soc. Jpn.* **80** (2011) 014702.
- 33) A. K. McMahan: *Phys. Rev.* **72** (2005) 115125.
- 34) H. Yamaoka, I. Jarrige, A. Ikeda-Ohno, S. Tsutsui, J.-F. Lin, N. Takeshita, K. Miyazawa, A. Iyo, H. Kito, H. Eisaki, N. Hiraoka, H. Ishii, and K.-D. Tsuei: *Phys. Rev. B* **82** (2010) 125123.
- 35) O. Gunnarsson and K. Schönhammer: *Phys. Rev. B* **28** (1983) 4315.
- 36) M. Yano, A. Sekiyama, H. Fujiwara, Y. Amano, S. Imada, T. Muro, M. Yabashi, K. Tamasaku, A. Higashiya, T. Ishikawa, Y. Ōnuki, and S. Suga: *Phys. Rev. B* **77** (2008) 035118.
- 37) N. E. Bickers, D. L. Cox, and J. W. Wilkins: *Phys. Rev. B* **36** (1987) 2036.
- 38) P. Bonville, J. A. Hodges, P. Imbert, D. Jaccard, J. Sierro, M. J. Besnus, and A. Meyer: *Physica B* **163** (1990) 347.
- 39) P. Bonville, J. Hammann, J. A. Hodges, G. Imbert, P. Jéhanno, M. J. Besnus, and A. Meyer: *Physica B* **171** (1991) 171.
- 40) G. Knebel, R. Boursier, E. Hassinger, G. Lapertot, P. G. Niklowitz, A. Pourret, B. Salce, J. P. Sanchez, I. Sheikin, P. Bonville, H. Harima, and J. Flouquet: *J. Phys. Soc. Jpn.* **75** (2006) 114709.
- 41) N. Andrei and J. H. Lowenstein: *Phys. Rev. Lett.* **46** (1981) 356.
- 42) V. T. Rajan: *Phys. Rev. Lett.* **51** (1983) 308.
- 43) E. D. Bauer, R. Chau, N. R. Dilley, M. B. Maple, D. Mandru, and B. C. Sales: *J. Phys.: Condens. Matter* **12** (2000) 1261.
- 44) J.-P. Rueff, S. Raymond, M. Taguchi, M. Sikora, J.-P. Itié, F. Baudelet, D. Braithwaite, G. Knebel, and D. Jaccard: *Phys. Rev. Lett.* **106** (2011) 186405.
- 45) H. Mukuda, T. Fujii, T. Ohara, A. Harada, M. Yashima, Y. Kitaoka, Y. Okuda, R. Settai, and Y. Ōnuki: *Phys. Rev. Lett.* **100** (2008) 107003.
- 46) Q. Si, S. Rabello, K. Ingersent, and J. L. Smith: *Phys. Rev. B* **68** (2003) 115103.
- 47) S. Watanabe and K. Miyake: *J. Phys. Soc. Jpn.* **79** (2010) 033707.
- 48) Y. Onishi and K. Miyake: *J. Phys. Soc. Jpn.* **69** (2000) 3955.
- 49) K. Miyake: *J. Phys.: Condens. Matter* **19** (2007) 125201.
- 50) S. Watanabe and K. Miyake: *J. Phys.: Condens. Matter* **23** (2011) 094217.
- 51) A. Kotani, T. Jo, and J. C. Parlebas: *Adv. Phys.* **37** (1988) 37.
- 52) A. Kotani and H. Ogasawara: *J. Electron Spectrosc. Relat. Phenom.* **60** (1992) 257.
- 53) A. Kotani: *Eur. Phys. J. B* **72** (2009) 375.